AUTHORS:
Sibongile M. Malunga[1]
Nhamo Chaukura[2]
Chiedza I. Mbiriri[3]
Willis Gwenzi[4]
Mambo Moyo[5]
Alex T. Kuvarega[6]

AFFILIATIONS:
[1]Chemistry Department, Bindura University of Science Education, Bindura, Zimbabwe
[2]Department of Physical and Earth Sciences, Sol Plaatje University, Kimberley, South Africa
[3]Department of Biological Sciences, Bindura University of Science Education, Bindura, Zimbabwe
[4]Biosystems and Environmental Engineering Research Group, Department of Soil Science and Agricultural Engineering, University of Zimbabwe, Harare, Zimbabwe
[5]Department of Chemical Technology, Midlands State University, Gweru, Zimbabwe
[6]Nanotechnology and Water Sustainability Research Unit, College of Engineering, Science and Technology, University of South Africa, Johannesburg, South Africa

CORRESPONDENCE TO:
Nhamo Chaukura

EMAIL:
nhamo.chaukura@spu.ac.za

DATES:
Received: 28 Apr. 2021
Revised: 16 Sep. 2021
Accepted: 21 Sep. 2021
Published: 27 Jan. 2022

HOW TO CITE:
Malunga SM, Chaukura N, Mbiriri CI, Gwenzi W, Moyo M, Kuvarega AT. Visible light photodegradation of methyl orange and *Escherichia coli* O157:H7 in wastewater. S Afr J Sci. 2022;118(1/2), Art. #10938. https://doi.org/10.17159/sajs.2022/10938

ARTICLE INCLUDES:
☒ Peer review
☐ Supplementary material

DATA AVAILABILITY:
☐ Open data set
☐ All data included
☒ On request from author(s)
☐ Not available
☐ Not applicable

EDITOR:
Jennifer Fitchett

KEYWORDS:
catalysis, environmental remediation, pollution, porous materials, wastewater, zeolite

FUNDING:
None

Visible light photodegradation of methyl orange and *Escherichia coli* O157:H7 in wastewater

Water pollution due to dyes and pathogens is problematic worldwide, and the disease burden is higher in low-income countries where water treatment facilities are usually inadequate. Thus the development of low-cost techniques for the removal of dyes and pathogens in aquatic systems is critical for safeguarding human and ecological health. In this work, we report the fabrication and use of a photocatalyst derived from waste from coal combustion in removing dyes and pathogens from wastewater. Higher TiO_2 loading of the photocatalyst increased the removal efficiency for methyl orange (95.5%), and fluorine-doping improved the disinfection efficacy from 76% to 95% relative to unmodified material. Overall, the work effectively converted hazardous waste into a value-added product that has potential in point-of-use water treatment. Future research should focus on upscaling the technique, investigating the fate of the potential of the photocatalysts for multiple reuse, and the recovery of TiO_2 in treated water.

Significance:

- The study provides a pathway for the fabrication of a value-added product from coal fly ash waste.
- The use of the proposed nanocomposite material for wastewater treatment represents a potentially affordable, simple, and sustainable technology for point-of-use water treatment.

Introduction

Dyes such as methyl orange and methylene blue are used in printing, pharmaceuticals and research laboratories, but the textile industry remains one of the most polluting industries that use dyes due to the large quantities of effluents discharged.[1] The World Bank estimates that the textile dyeing industry contributes 20% of all industrial wastewater pollution globally.[2] Azo dyes account for up to 70% of all textile dyes produced, and hence constitute a major component (2–20%) of wastewater effluents discharged from textile industries.[3,4] Due to their intricate aromatic molecular structure and synthetic origin, dyes and pigments are mostly non-biodegradable.[1] Consequently, they cause water pollution, even at very low concentrations. Moreover, dyes decrease light penetration and thus reduce photosynthesis in aquatic plants.[5] Dyes may also contain toxic metals, either within their structure or through complexation in the environment. Hence, their removal in wastewater has been a subject of interest in recent years.

The presence of coliforms, in particular *Escherichia coli*, in water indicates faecal contamination; therefore *E. coli* is one of the most common and important indicator organisms of water safety. Some strains, of which O157:H7 is representative, cause sporadic outbreaks of severe food and waterborne disease. *E. coli* produces a shiga toxin which can cause severe enteric infection, resulting in diarrhoea, haemorrhagic colitis, and haemolytic-uremic syndrome in humans.[6] One key factor in reducing or eliminating such diseases lies in providing safe water, especially to isolated communities where centralised water supplies are limited.

Methods currently used for the removal of dyes include chemical coagulation, biodegradation, flocculation, precipitation, reverse osmosis, photocatalysis, adsorption, ionising and gamma radiation.[7] Recent developments in nanotechnology have led to the use of carbon-based and metal oxide nanocomposites to remove organic compounds.[8,9] However, these techniques have high capital and maintenance costs, and produce secondary pollutants through the generation of sludge, while oxidation processes may produce metabolic products that pose public health risks.[10] Greener and more cost-effective methods such as dye solubilisation using natural surfactants or biosurfactants have been recently proposed.[11,12] However, the methods work only with ionic dyes such as Congo Red, and their efficiency with non-ionic surfactants is limited.[11] Furthermore, wastewater treatment plants are not adequately equipped to remove dyes, especially where they are based on conventional methods. Therefore, there is need to develop innovative wastewater treatment technologies which are economically feasible, easy to operate and maintain, effective, and which allow for materials to be recovered and reused.[13]

Zeolites, which are aluminosilicate materials, are one of the most extensively used adsorbents due to their high contaminant removal efficiency arising from a large surface area.[14] The cost of natural zeolites is high, and becomes even higher when synthetic compounds are used. Fly ash (FA), a solid residue from the combustion of coal, is produced in large quantities in several developing countries, where it is stockpiled or disposed of in non-engineered landfills. Such poor disposal practices pose human and ecological health risks, and pollution due to discharged FA has been documented.[15] Globally, attempts have been made to convert FA into value-added products such as synthetic zeolites.[16] Thus, the overall environmental footprint and cost of FA-based zeolites is lower than that of natural zeolites or those developed from the precursors.

Advanced oxidation processes are a recent technology in the treatment of wastewater.[17] Of all the advanced oxidation processes, semiconductor photocatalysts are an interesting option in removing dyes because they can completely mineralise dyes at room temperature and pressure, via oxidation using light energy, and they can withstand the toxicity of dyes.[18] Among the photocatalysts, TiO_2 is most commonly used because it is cheap, non-toxic, thermodynamically and photo-chemically stable, works over a wide pH range, and its band edges are aligned to the redox potential of water.[17] Consequently, a number of studies have investigated photodegradation

using TiO_2-based nanoparticles.[8,19,20] The application of unmodified TiO_2 as a photocatalyst is limited by its wide band gap (3.2 eV), electron-hole recombination, and low absorption of visible light.[8] The high band gap in TiO_2 results in a reduction of photo-efficiency. Accordingly, dopants such as C, N, and F have been introduced to narrow the band gap.

TiO_2-zeolite nanocomposites have been studied for the removal of dyes in industrial effluent.[5,21] Zeolites can be cheaply obtained from FA. The conversion of FA into zeolites, and their subsequent use for contaminant removal, minimises the health risks associated with poor disposal of FA, while providing novel materials for wastewater treatment. The capacity of zeolites to remove contaminants can be enhanced by coupling to photocatalysts to produce hybrid materials, so that adsorption occurs on the zeolite while the photocatalyst degrades the pollutant.[21,22] In this study, we sought to improve the photo-efficiency of TiO_2 photocatalysts by using low-cost zeolites as support structures for doped TiO_2 in the photodegradation of methyl orange (MO) and *E. coli* in aqueous solution using a custom-made photocatalytic reactor. Although MO and *E. coli* do not always coexist in the natural aquatic environment, this work proves the case of the removal of organic compounds and pathogenic organisms. Most previous research has demonstrated the photodegradation of either a model dye compound or a model pathogen species separately. Moreover, they use photocatalysts synthesised from commercial reagents, which are expensive. Because it uses waste feedstock for the synthesis of photocatalysts, and mimics solar radiation in the photodegradation process, this is an affordable and sustainable innovative approach with immense potential in point-of-use water-treatment devices. Although the TiO_2 photocatalysts are likely to persist and cause pollution in treated water, their recovery was not investigated in this study. Specifically, the study aimed at: (1) synthesising a low-cost photocatalyst derived from fly ash, TiO_2, and fluorine, and (2) evaluating the photocatalytic behaviour of the materials in the degradation of MO and *E. coli*.

Materials and methods

Ethical considerations

Before carrying out this work, ethical clearance was provided based on the proposed handling of hazardous chemicals and data generation, processing, and storage. This ensured safe procedures were followed in handling chemicals and other potentially hazardous materials. The handling and disposal of *E. coli* was according to strict procedures that prevented contamination. Permission was obtained prior to sampling FA from a local power plant. Protocols for data generation, processing, storage, and sharing were followed to ensure integrity and validity of the findings.

Materials

Chemical reagents used included titanium (IV) isopropoxide (TTIP) (97%), 2-propanol (99.7%), formic acid (85%), NaOH (98%), trifluoroacetic acid (purity >97%), MO (85%) and HCl (30–33%). All the chemicals were of analytical reagent grade purchased from either Sigma-Aldrich, Merck, or Glassworld (Berlin, Germany). Except in the study of the degradation of *E. coli* where Ringer's solution was used, deionised water was used to prepare solutions. FA was obtained from Harare Thermal Power Station, and *E. coli* 0157:H7 was obtained from Sigma-Aldrich. A custom-made photocatalytic reactor was fabricated from 5-m-long light emitting diode strips (60 LED/m, 4.8 W, 12 V DC, luminous flux 360 lm/m, and colour temperature 3000 K) wrapped around a 1-L glass beaker and held in place using tape (Figure 1). Preliminary tests conducted using TiO_2 and methylene blue dye showed that the intensity of the light output can be tuned to the desired level by controlling the luminance. In this work, white light at 80% luminance was used for all experiments.

Preparation of photocatalysts

TiO_2

The sol-gel method was used to prepare TiO_2 nanoparticles with TTIP as a precursor. Briefly, TTIP (10 mL) was dissolved in 2-propanol (50 mL) and stirred to get a homogeneous solution. Under continuous stirring, formic acid (10 mL) was added dropwise for 60 min to hydrolyse the mixture. The resulting TiO_2 sol was left to age for 24 h at room temperature. The dry TiO_2 gel was placed in a muffle furnace and calcined at 450–500 °C for 3 h.

Zeolitic fly ash

Zeolites were synthesised from FA via hydrothermal synthesis using NaOH to produce zeolite fly ash (ZFA).[23] Zeolitic materials have been prepared previously from the same FA using a similar method and

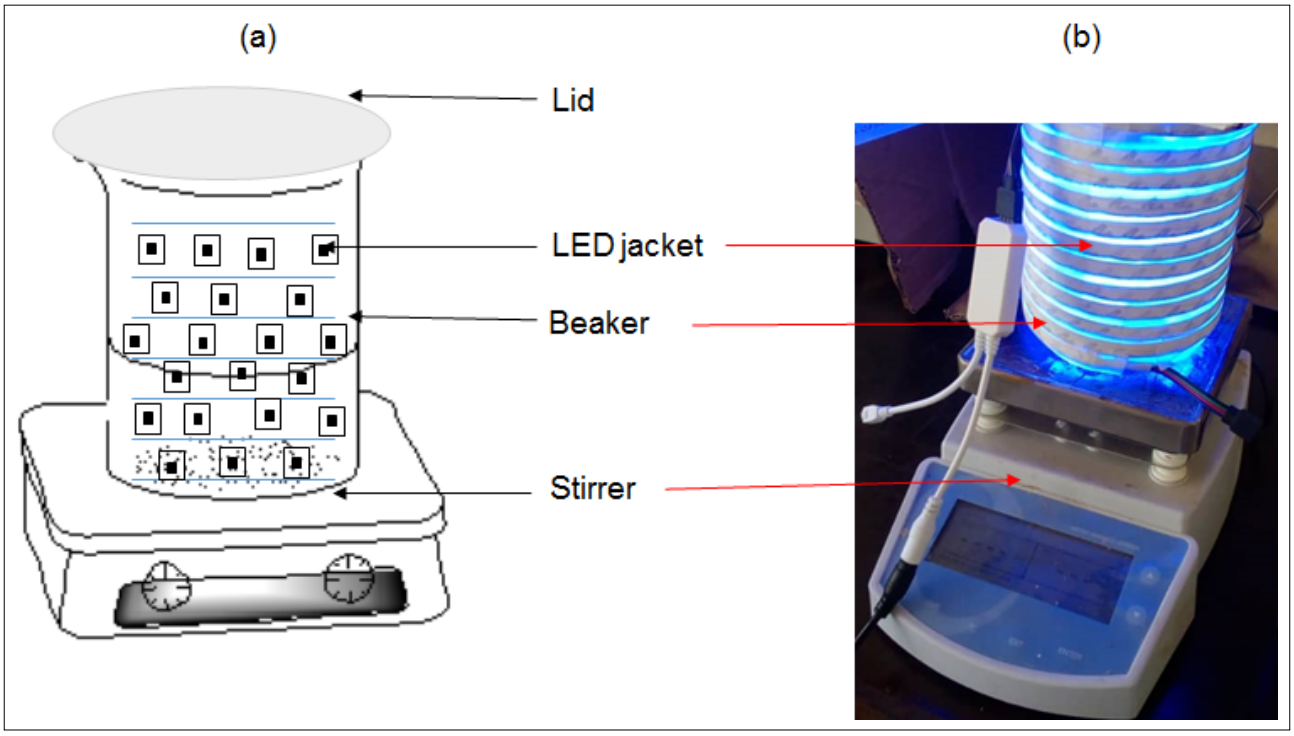

Figure 1: The custom-made photocatalytic reactor showing (a) the sketch, and (b) the digital image of the reactor.

successfully used to remove metals in acid mine drainage.[24] In brief, FA was dried in an oven at 70 °C. NaOH pellets were added to the dry FA in the ratio 1:12 (w/w), and the mixture was ground and mixed thoroughly. The mixture was fused at 550–600 °C for 1 h in a muffle furnace, after which it was cooled and ground again. To the resulting powder was added deionised water (400 mL) and this mixture was stirred at room temperature overnight. This mixture was then placed in an oven to cure at 55 °C for 4 days to allow crystallisation to occur. The solid was separated from the liquid phase by filtration using No. 1 Whatman filter paper. The resulting ZFA was washed twice with distilled water, dried in an oven at 80 °C for 12 h, and milled to pass through a 250-μm sieve.

TiO_2-ZFA nanocomposites

A one-pot acid catalysed sol-gel synthesis method was used to prepare TiO_2-ZFA nanocomposites. In this method, ZFA of particle size 75 μm and mass 24.5 g was added to 2-propanol (50 mL), followed by 30 min of stirring at 40 °C. Different volumes of TTIP (Table 1) were added to the mixture to give 5%, 7% and 10% TiO_2 (w/w) followed by stirring for a further 30 min. Then formic acid (10 mL) was added dropwise under continuous stirring for 30 min until a white sol-gel was observed. This sol-gel was allowed to age for 24 h at room temperature and then dried in an oven at 80 °C for 10 h. The sample was then ground to pass through a 250-μm sieve, and calcined at 450 °C for 4 h in a muffle furnace.

Table 1: Preparation of TiO_2-ZFA photocatalysts

Sample	TTIP (mL)	2-propanol (mL)	Formic acid (mL)	ZFA (g)
5% TiO_2-ZFA	5	50	10	24.5
7% TiO_2-ZFA	7	50	10	24.5
10% TIO_2-ZFA	10	50	10	24.5

F-doped TiO_2 and F-doped TiO_2-ZFA photocatalysts

F-doped TiO_2 (F-TiO_2) was prepared using a two-step sol-gel method.[25] Specifically, TTIP (10 mL) was dissolved in 2-propanol (50 mL) and vigorously stirred for 10 min to make solution A. Trifluoroacetic acid (0.5 mL) was mixed with 2-propanol (30 mL), formic acid (10 mL), deionised water (10 mL) and HCl (3 mL) and continuously stirred for 30 min to make solution B. This solution was added dropwise to solution A and continuously stirred for 30 min until a white sol-gel was observed. The sol-gel was aged for 24 h, oven-dried overnight at 50 °C, ground to pass through a 250-μm sieve, and calcined at 450 °C for 4 h in a muffle furnace. F-doped TiO_2-ZFA (F-TiO_2-ZFA) was prepared in the same way except the precursor was TiO_2-ZFA, and CF_3CO_2H was used instead of formic acid.

Characterisation of photocatalysts

pH_{zpc} and ash content

The pH_{zpc} was used as a proxy for surface charge, and it was determined to elucidate the solid-liquid interfacial charge interactions between the photocatalysts and MO molecular surfaces.[26] Determination of pH_{zpc} was performed following the pH-drift method.[27] The ash content was determined from the mass difference before and after igniting the samples at 750 °C for 4 h.

Fourier transform infrared spectroscopy

To determine the surface functional groups on the photocatalysts, infrared spectra were recorded using a Fourier transform infrared (FTIR) spectrometer (Analytical® Technologies Limited, Infra 3000A, India). The samples were prepared using the KBr pellet method with a sample/KBr ratio of 1:40 to allow the samples to be infrared transparent. The spectra were recorded using 32 scans in the range 4000–400 cm^{-1} with a resolution of 4.

Diffuse reflectance UV-Vis spectroscopy

Diffuse reflectance spectroscopy UV-Vis spectra of the photocatalysts were measured using a UV-Vis near-infrared spectrophotometer[22] (Lambda 650S, PerkinElmer, Johannesburg, South Africa) equipped with deuterium and tungsten lamps as the UV-Vis near-infrared radiation sources. The reflectance (*R*) for each sample was measured in the range 250–800 nm using the 150-mm sphere reflectance method. A slit width of 4 mm, a 0.2-s photomultiplier response, and reflectance blank of $BaSO_4$ were used. From the UV-Vis data, an absorption coefficient was obtained in the form of the Kubelka–Munk function *[F(R)]*[25,28], which was used to predict reflectance based on radiation transfer (Equation 1):

$$F(R) = \frac{(1-R)^2}{2R} \qquad \text{Equation 1}$$

Using the equation of Tauc (Equation 2), the band gap (E_g) for the different photocatalysts was estimated.[29] Values of E_g were determined at the point of the horizontal intercept from plots of $[h\upsilon \times F(R)]^{1/n}$ against $h\upsilon$.

$$(h\upsilon \times F(R))^{\frac{1}{n}} = A(h\upsilon - E_g)^n, \qquad \text{Equation 2}$$

where *h* is Plank's constant (6.626 x 10^{-34}), *v* is frequency of radiation, *c* is the speed of light (3.0 x 10^8 m/s), *n* is the numerical value of electronic transitions and is equal to 2 for TiO_2.

Surface morphology and crystallinity of the photocatalysts

Scanning electron microscopy (SEM) was used to obtain information on the surface morphology of the photocatalyts.[15] Micrographs were obtained from a SEM microscope (Tescan, Vega 3, Brno, Czech Republic). Samples were prepared by placing powdered samples on an adhesive carbon tape stuck to a sample holder and then sputter-coating with 15 μm gold film; samples were observed under a microscope at 50 μm magnification. The crystallinity of the photocatalysts was measured using a powder X-ray diffraction spectrometer[19,22] (D2 Phaser, Bruker, Billerica, MA, USA) fitted with a Cu X-ray source at 1.5418 Å, and operated in the continuous position-sensitive detector fast-scan mode.

Preparation of MO solutions and E. coli *contaminated water*

A 100 mg/L stock solution of synthetic wastewater was prepared by dissolving a known mass of MO dye in deionised water. From this, working solutions (1, 2, 3, 4, 5 mg/L) were prepared by serial dilution. *E. coli* 0157:H7, a commonly used indicator organism, was selected as the model microorganism representing potentially pathogenic organisms occurring in water and wastewaters. The initial concentration of *E. coli* in the synthetic wastewater was 3.8 x 10^8 CFU/mL; the concentration was enumerated initially and at hourly intervals for 3 h thereafter.[30] HiCrome™ *E. coli* agar, a selective medium that allows for the growth of *E. coli*, and nutrient agar for subsequent enumeration, were used. *E. coli* cell cultures were made to the sixth dilution using Ringer's solution, and the cultures were plated on duplicate nutrient agar plates for each dilution. The agar plates were then incubated at 37 °C for 48 h.

Evaluation of the photocatalytic activity of photocatalysts

Photodegradation experiments were performed using a custom-made photocatalytic reactor to evaluate the effect of contact time on the photodegradation process. The kinetics of the photodegradation of MO were studied using F-doped photocatalysts owing to their superior photocatalytic properties. The photodegradation studies were carried out using 100 mL of synthetic wastewater at 25 °C, at pH 7.2, a photocatalyst dosage of 500 mg, a dye concentration of 2 mg/L, and contact time of -60, 0, 60, and 120 min in a 150 mL beaker, following a variation of the method reported by Mukonza et al.[25] To eliminate the interference of leftover photocatalyst in absorbance readings, a blank experiment of distilled water and photocatalyst was set up. All samples were stirred in the dark for 1 h under room temperature (25±1 °C) to attain absorption equilibria before being irradiated with visible light in the photocatalytic reactor.

The concentrations of MO before (C_0) and after (C_t) photodegradation experiments were determined based on UV-Vis absorbance spectra. Samples (4 mL) were drawn at 1 h intervals using a 10-mL syringe and filtered through a 0.45-μm filter. The aliquots were centrifuged and the residual concentration of MO in the supernatant was measured at 460 nm using a UV-Vis spectrophotometer (Spectroquant® Pharo 300). The dye removal (r) was computed using Equation 3[31]:

$$r = \frac{C_0 - C_t}{C_0} \times 100 \quad \text{Equation 3}$$

The order of reaction for the photocatalytic degradation of MO was confirmed using the linearised Langmuir–Hinshelwood model (Equation 4)[29]:

$$\mathrm{h}\left(\frac{C_0}{C_t}\right) = k_{app} t\,, \quad \text{Equation 4}$$

where k_{app} is the apparent reaction rate constant.

Evaluation of the antimicrobial activity of the photocatalysts

To determine the individual effects of visible light irradiation and adsorption on the photodegradation of *E. coli*, experiments were conducted in triplicate under the following conditions: (1) in the presence of photocatalysts under dark conditions, (2) in the absence of photocatalysts under light irradiation, (3) in the absence of photocatalysts under dark conditions and (4) in the presence of catalysts and light irradiation. To reduce growth before assaying, water samples were refrigerated at <4 °C. Monitoring *E. coli* numbers was indicative of the quality of the wastewater and the efficacy of the disinfection process. From these data, the disinfection rate was calculated using Equation 3. Samples from disinfection experiments were plated on nutrient agar in duplicate, and incubated at 37 °C for 48 h. Thereafter, colonies were counted and viable cell concentrations determined.[32]

Data analysis

One-way analysis of variance (ANOVA) was used to determine the individual effects of the photocatalysts and experimental factors on MO and *E. coli* removal after testing the data for normality and homogeneity of variance. Data that violated the ANOVA assumptions were either transformed or analysed using non-parametric statistical tests. Regression analysis was used to test the degree of fit of kinetic models to the experimental data based on the coefficient of determination. All statistical analyses were done at a probability level (p) of 0.05 using SPSS statistical software.

Study limitations

The limitations of this work were: (1) the removal of MO and *E. coli* from synthetic wastewater samples rather than real wastewater, and (2) evaluation of pollutant removal at laboratory scale. Hence, the following could not be adequately addressed in the current study: (1) potential interactions among contaminants, and (2) effects of typical concentrations occurring in wastewaters. Moreover, no experimental work was conducted to investigate regeneration potential.

Results and discussion

Characteristics of TiO_2-ZFA and F-TiO_2-ZFA nanocomposites

pH_{zpc} and ash content of photocatalyst

While TiO_2 had no significant effect on the pH_{zpc}, all the F-doped TiO_2 photocatalysts shifted towards lower pH_{zpc} as the TiO_2 content increased (Table 2). For the photocatalysts, a high pH_{zpc} is associated with a positive surface charge, while low pH_{zpc} is associated with a negative surface charge.[26] Surface charge affects the agglomeration of the nanoparticles and their stability in suspension, with a more negative surface charge leading to less particle agglomeration.[26] The results showed that the ash content significantly (p=0.05) decreased with dopant loading. The ash content of TiO_2 was lowest, while ZFA had the highest ash content. Generally, ash content is an indication of the amount of inorganic material bound in the physical structure of the nanocomposites.[22] The ash content for TiO_2-ZFA photocatalysts was not significantly different (p>0.05), and averaged 85%, whereas F-TiO_2-ZFA photocatalysts averaged 72%. As expected, the presence of ZFA increases ash content, suggesting a high load of inorganic elements.

Table 2: Physico-chemical parameters of the photocatalysts

Photocatalyst	pH_{zpc}	Ash (%)
TiO_2	7.5±0.1	5±1
ZFA	7.0±0.1	98±3
5% TiO_2-ZFA	8.1±0.2	89±2
7% TiO_2-ZFA	8.1±0.1	85±2
10% TiO_2-ZFA	8.2±0.1	82±3
10% F-TiO_2-ZFA	6.6±0.1	76±1
20% F-TiO_2-ZFA	6.4±0.1	72±2
30% F-TiO_2-ZFA	6.1±0.1	69±1
100% F-TiO_2	5.4±0.1	10±1

Surface functional groups

The FTIR spectra for ZFA and TiO_2-ZFA resemble those for zeolites (Figure 2). The broad peaks at ~3400 cm^{-1} were attributed to -OH vibrations of silanol groups (Si-OH), which are formed from the interaction of -Si groups in the ZFA with water molecules.[7] The small peaks at ~1600 cm^{-1} are characteristic of the -OH bending vibrations in water molecules linked to zeolite particles.[1] All spectra for the F-doped photocatalysts showed broad O-H stretching peaks in the range 3200–3500 cm^{-1}, which were ascribed to adsorbed moisture. The presence of the O-H functional groups enhances the photocatalytic activity because holes generated under irradiation trap O-H groups to produce OH• radicals, which reduce electron-hole recombination.[5] The intensities of the O-H bond peak increased with increasing F-TiO_2 loading, suggesting possible higher photocatalytic activity for the 30% F-TiO_2 than for photocatalysts at lower TiO_2 loadings. Sharp Ti-O-Si peaks were observed between 900 cm^{-1} and 1000 cm^{-1}. Similar peaks were reported in a previous study, and were attributed to the Ti-O-Si bonds formed when Ti was introduced into the ZFA structure.[33] However, another study attributed the peaks to the Al-O-Al or Si-O-Si bonds found in the AlO_4 and SiO_4 tetrahedra in the ZFA structure.[21] The ZFA-doped photocatalysts are expected to have both these functional groups. The C=O stretch in the range 1760–1690 cm^{-1} suggests the presence of some residual CF_3CO_2H used for doping the material.[34] The broad symmetrical peak around 750 cm^{-1} was ascribed to the Ti-O-Ti bond, while the peak at 1100 cm^{-1} suggests the presence of the Ti-O-C bond. The presence of the Ti-O-C peak shows some chemical bonding interactions between the TiO_2 nanoparticles and the ZFA.[1] Comparing spectra for TiO_2-ZFA and F-TiO_2-ZFA shows F-doping increased the intensities of all the O-H peaks, suggesting F-doping potentially enhances photocatalytic activity.[19] The peak at 2347 cm^{-1} only appears in F-doped samples, and points to traces of residual C-C=O groups from TTIP precursors and solvents used during synthesis. The C-F bond around 1400 cm^{-1} confirms the presence of F in the F-TiO_2-ZFA photocatalysts, and thus successful F-doping.[34]

Surface morphology

The surface morphology of TiO_2, ZFA, TiO_2-ZFA and F-TiO_2-ZFA was characterised by heterogeneous and rough surfaces (Figure 3). Aggregates of TiO_2 nanoparticles showed characteristic dispersed near-spherical particles with a rash-like appearance (Figure 3a).[1,22,32] ZFA showed larger particles than TiO_2 with irregular-shaped edges (Figure 3b). Particles in the nanocomposite photocatalysts were of different irregular shapes with a broad size distribution (Figure 3c, d). After being introduced into the photocatalyst, particles of ZFA formed

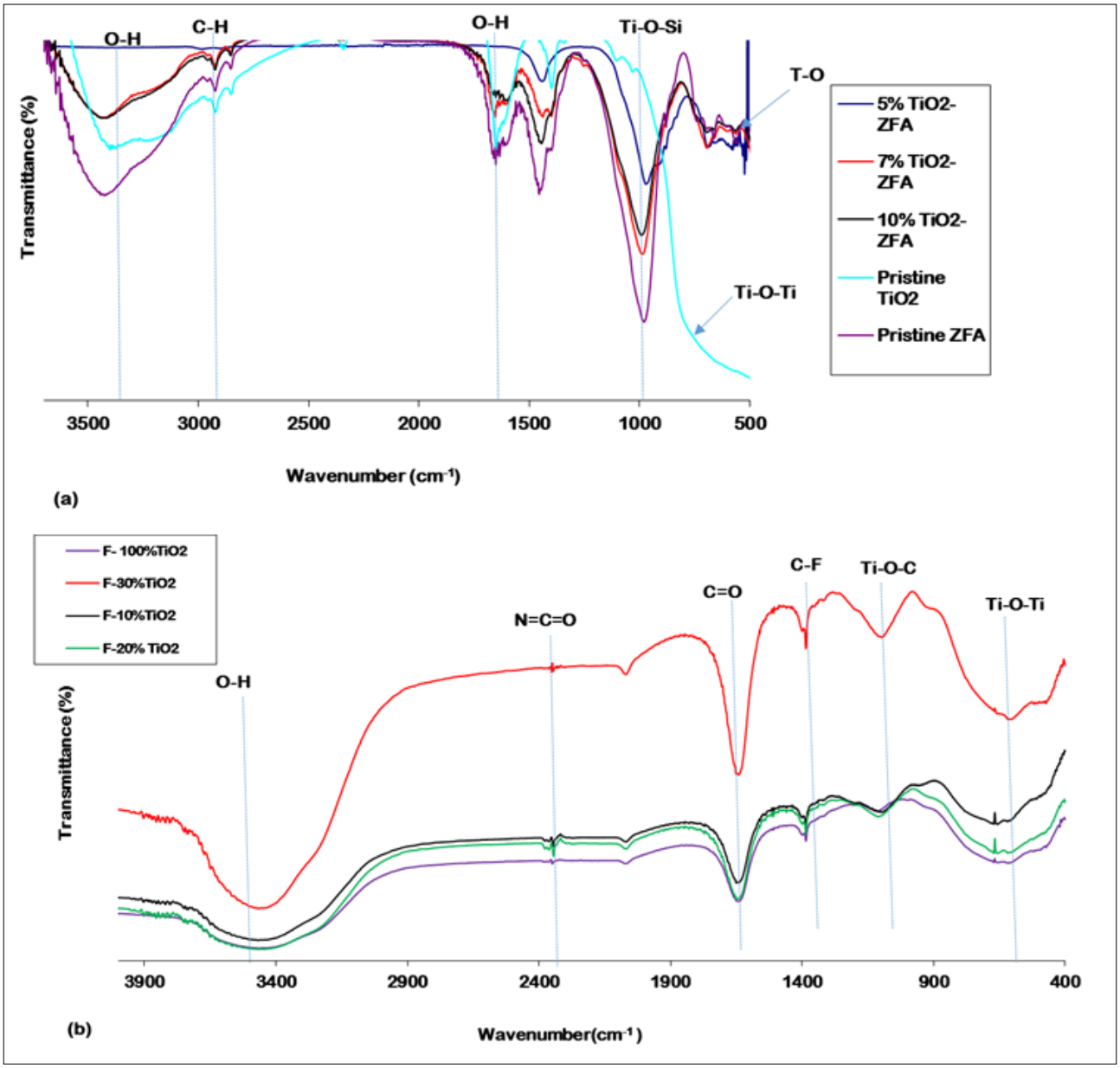

Figure 2: Fourier transform infrared spectra for TiO_2, ZFA and TiO_2-ZFA photocatalysts, F-TiO_2, and F-TiO_2-ZFA photocatalysts.

plate-like units with an irregular and rough surface with numerous microsized cavities (Figure 3c). The estimated average sizes of the TiO_2-ZFA and F-TiO_2-ZFA particles were in the range of several hundred nanometres. This big particle size could be due to the presence of the microsized ZFA particles. Images of TiO_2-ZFA and F-TiO_2-ZFA show TiO_2 nanoparticle agglomerates embedded onto ZFA particles (Figure 3c, d). Because of the smaller quantity of TiO_2 relative to ZFA, most of the TiO_2 particles were covered and hidden under the ZFA particles. The SEM images suggest the TiO_2 nanoparticles were immobilised on the external surface of the ZFA particles and not in the pore structures and voids of the ZFA particles.[32] From these images, it is clear that the morphology of the precursors was transformed through the modification via synthesis. Overall, the surface morphologies of the photocatalysts are suitable for the photodegradation of MO subsequent to adsorption, and provide a heterogeneous surface for accommodating *E. coli*.

Crystallinity of the photocatalysts

Unmodified TiO_2 showed X-ray diffraction peaks at $2\theta = 25°$, 38°, and 48°, which are characteristic of the anatase phase (Figure 4).[5] The spectra for ZFA showed multiple crystalline and amorphous regions. This is expected from the wide range of organic carbon and metal compounds that constitute FA.[19,35] These characteristics were inherited by TiO_2-ZFA, which showed an increased crystallinity owing to the presence of TiO_2. The organic matter in the photocatalyst nanocomposite is beneficial for adsorption along with zeolitic porous properties, while the TiO_2 is key to the photocatalytic properties.[5]

Photoactive properties

Diffuse reflectance spectroscopy UV-Vis spectra showed the photoactive properties of the various photocatalysts (Figure 5a, b). Compared to those for TiO_2 and F-TiO_2, the spectra for the F-TiO_2-ZFA photocatalysts have absorbance in the visible light region and a red shift. For TiO_2, the band gap was estimated to be 3.2 eV, which was within the 3.0–3.2 eV range reported in the literature.[36] For F-TiO_2, there was a slight shift in the band gap energy to 2.8 eV, which is comparable to the 2.75 eV reported in previous studies.[19] F-TiO_2-ZFA samples showed a 63–72% decrease in band gap relative to TiO_2, while TiO_2-ZFA samples showed a 31–38% band gap narrowing (Table 3). In summary, increasing the dopant loading into the TiO_2 led to a decrease in the band gap energies. F-TiO_2-ZFA

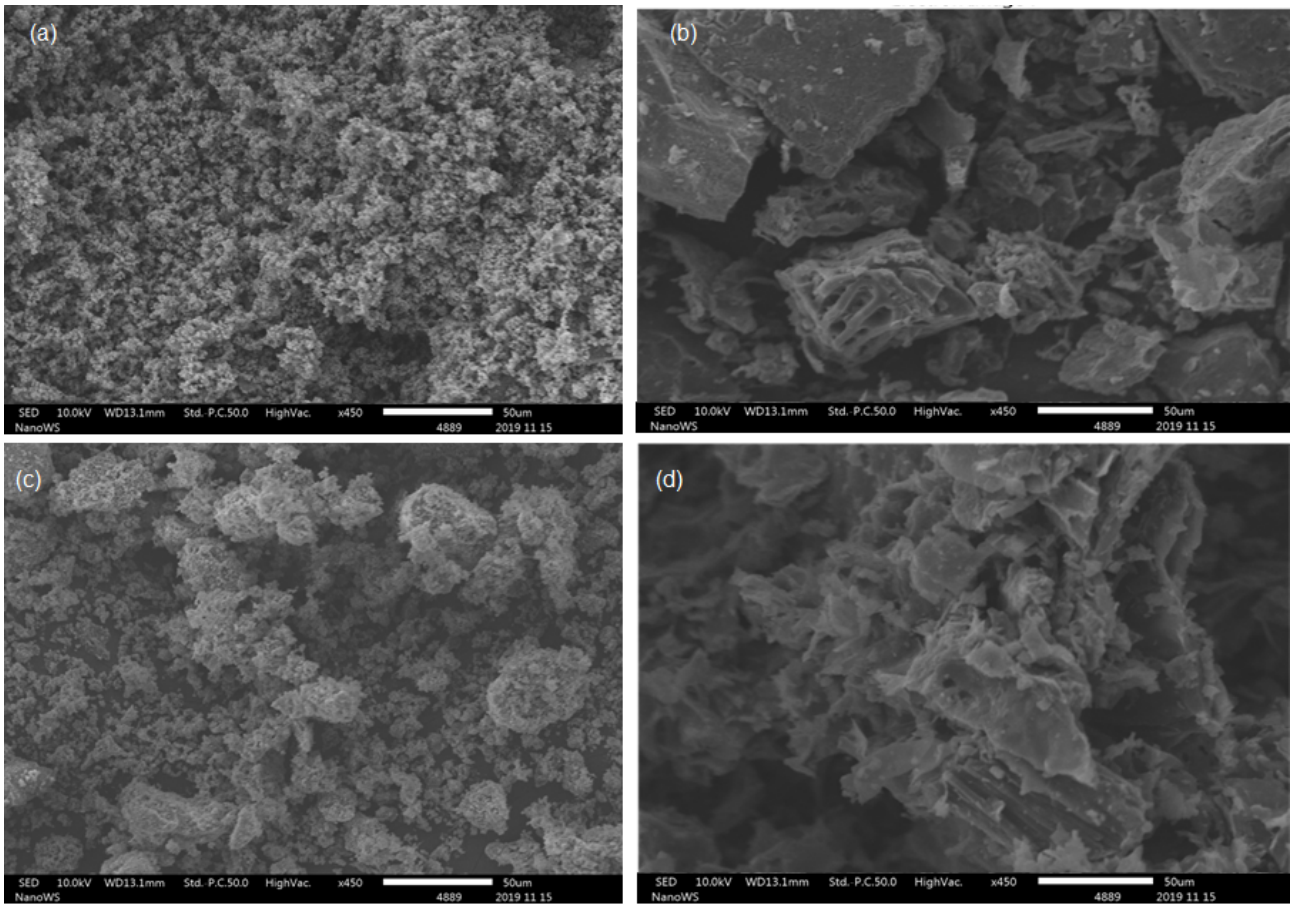

Figure 3: Scanning electron microscopy images for (a) TiO_2, (b) ZFA, (c) 10% TiO_2-ZFA, and (d) 30% F-TiO_2-ZFA.

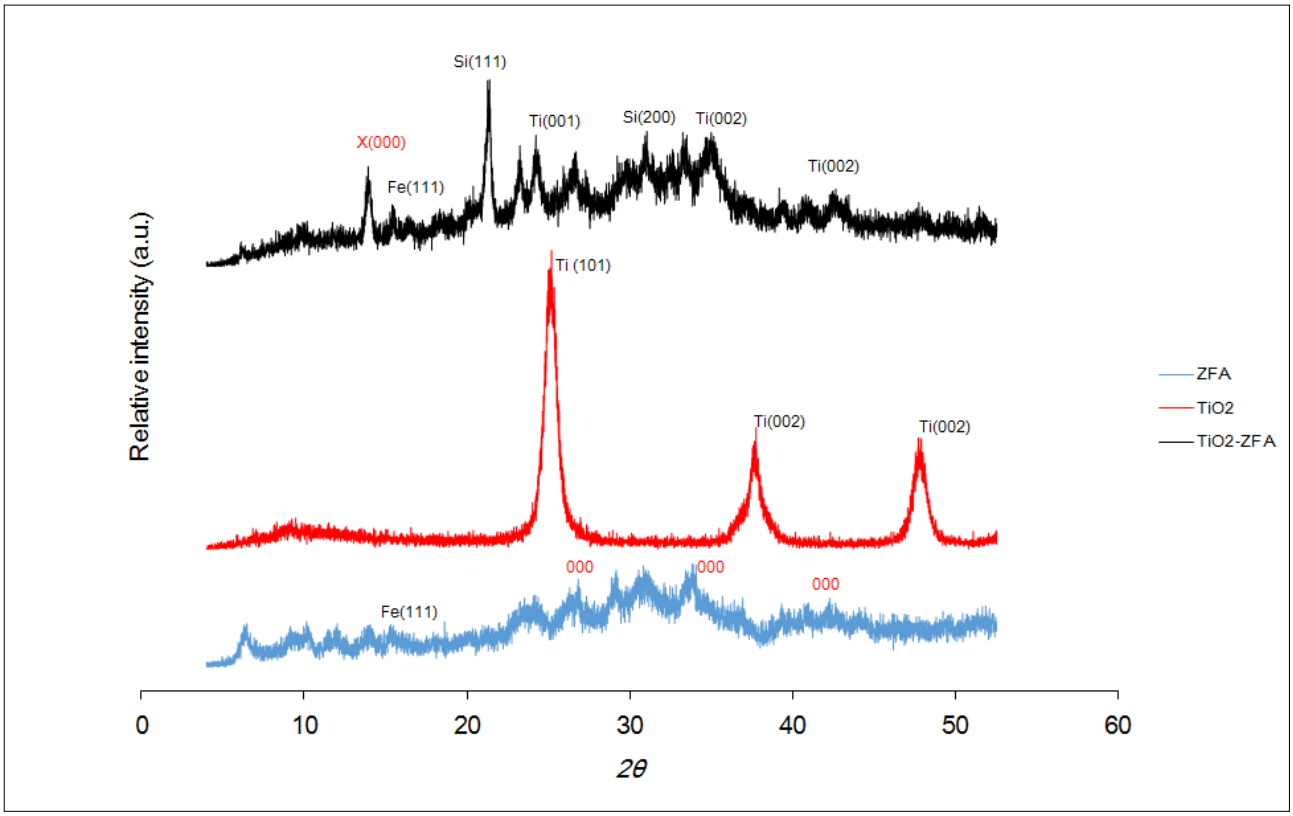

Figure 4: X-ray diffraction spectra for TiO_2, ZFA, and 10% TiO_2-ZFA.

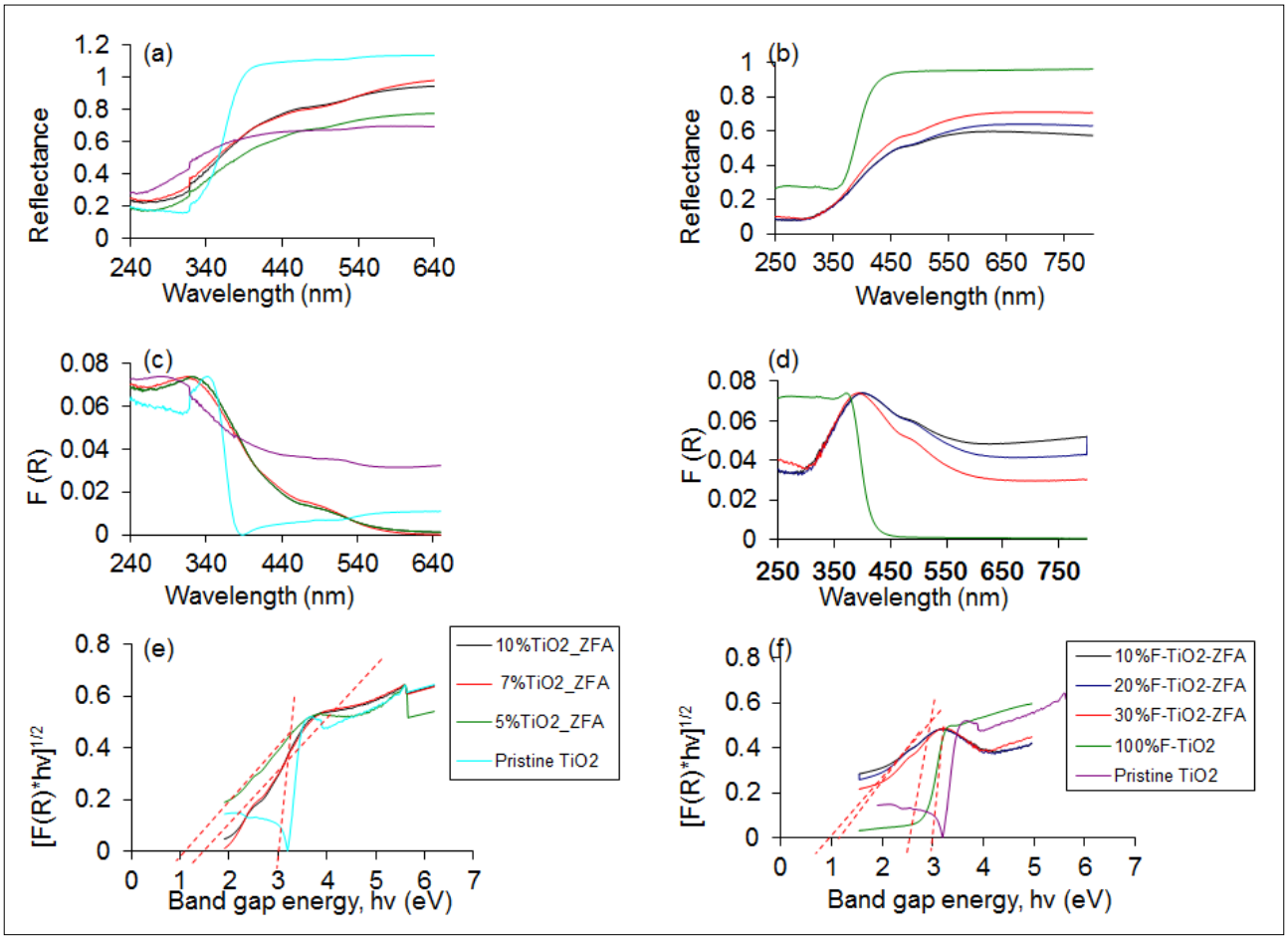

Figure 5: Diffuse reflectance UV-Vis spectra for (a) TiO_2, 5–7% TiO_2-ZFA and (b) TiO_2, 10–30% TiO_2-ZFA. Kubelka–Munk function plots for (c) TiO_2, 5–7% TiO_2-ZFA and (d) TiO_2, 10–30% TiO_2-ZFA. Tauc plots for (e) TiO_2, 5–7% TiO_2-ZFA and (f) TiO_2, 10–30% TiO_2-ZFA.

samples showed increased absorption intensities extending to the near-infrared region of the electromagnetic spectrum (Figure 5a, b). This increase is due to the narrowing of the band gap caused by introduction of ZFA and F. Although the intention of using ZFA was as an immobiliser for TiO_2 nanoparticles, Tauc plots show that ZFA also reduced the band gap for TiO_2. During calcination, some of the constituents of ZFA, such as carbon, may become potential TiO_2 dopants. It thus appears that the TiO_2 in F-TiO_2-ZFA samples was co-doped, hence the significant narrowing of the band gap. Given its off-white colour, ZFA will absorb in the entire visible region, thus enhancing the visible light absorption of the nanocomposite. Similar findings were observed for F and Sm co-doped TiO_2 nanocomposites.[25] The absorption edge for TiO_2-ZFA was also red-shifted into the visible light region of the electromagnetic spectrum. The introduction of ZFA and F^- introduced impurities, which in turn introduced intra-band gap energy states between the valence band and conduction band of TiO_2. The radius of the F^- anion (131 pm) is smaller than that of the O^{2-} (140 pm), hence it is possible that F^- occupies substitutional doping sites, replacing O^{2-} and resulting in a 2p energy sub-state above the valence band.[20] In contrast, the radii of tetrahedral $[SiO_4]^{4-}$ and $[AlO_4]^{5-}$ in ZFA is much bigger than that of O^{2-}, and more likely to occupy the interstitial doping sites.[37]

Kinetics of the photodegradation of MO

Unmodified TiO_2 had the least photocatalytic activity, and the fractional degradation of MO was the lowest (13.5%) (Figure 6a). The rate of degradation was fast in the first 60 min for all the doped photocatalysts. Beyond 60 min, there was a slight decrease in degradation. Hence optimum visible light irradiation time appears to be 60–120 min. Previous research reported that TiO_2-based photocatalysts are a good choice for the degradation of organic dyes such as Rhodamine B and methyl orange.[8,20]

Table 3: Indirect band gap energy estimates and calculated absorption wavelengths for different TiO_2-ZFA and F-TiO_2-ZFA samples

Sample	Indirect band gap (eV)	*Estimated λ (nm) $\left(\lambda = \frac{h}{E_g}\right)$
Pristine TiO_2	3.2	387.5
5% TiO_2-ZFA	2.2	563.6
7% TiO_2-ZFA	2.0	620.0
10% TiO_2-ZFA	2.0	620.0
10% F-TiO_2-ZFA	0.9	1377.8
20% F-TiO_2-ZFA	0.9	1377.8
30% F-TiO_2-ZFA	1.2	1033.3
100% F-TiO_2	2.8	442.9

The photocatalytic degradation of MO using 100% F-TiO_2 was 52% higher than TiO_2. This is possibly a result of the band gap narrowing for the 100% F-TiO_2, which is more aligned to absorption of radiation in the visible region than TiO_2. The order of the degradation was: TiO_2 (13.5%)<100% F-TiO_2 (56%)<10% F-TiO_2-ZFA (59.5%)<20% F-TiO_2-ZFA (69%)<10% TiO_2-ZFA (88%)<30% F-TiO_2-ZFA (95.5%) (Figure 6a). In general, reducing the F-loading in the photocatalysts resulted in diminished photocatalytic activity, possibly due to increasing band gap energy. Previous studies have reported that the introduction of F into TiO_2 results in an increase in photocatalytic activity due to the

reduction of the band gap.[25] Fluorine substitution has been reported to reduce the electron-hole recombination rate due to the charge compensation between F^- and Ti^{4+}.[38] Moreover, F-doping also creates oxygen vacancies that serve as active sites for the formation of OH• radicals, which in turn enhance photoactivity.[39]

The photocatalytic degradation of MO is a pseudo-first-order reaction as confirmed by the linear transforms of $ln(A_0/A_t)$ against t ($0.80<r^2<0.93$) from which rate constants were computed (Figure 6b). The photocatalyst 30% F-TiO_2-ZFA had the highest apparent pseudo-first-order rate constant (k_{app}) of 11.9 x 10^{-3} min^{-1} compared to 8 x 10^{-3} min^{-1} for 20% F-TiO_2-ZFA and 5.3 x 10^{-3} min^{-1} for 10% F-TiO_2-ZFA. The rate constant for TiO_2 was the lowest at 2.5 x 10^{-3} min^{-1}. The degradation rate increased with higher catalyst loading, indicative of the corresponding increases in the available catalytic and adsorption sites, resulting in more MO molecules being adsorbed and degraded. Previous studies have shown that F-TiO_2 has a higher rate constant (43.3x10^{-3} min^{-1}) compared to TiO_2 (4.2 x 10^{-3} min^{-1}).[38]

The difference in performance of the photocatalysts may be because of the difference in band gaps. The band gap for 10% TiO_2-ZFA (2.0 eV) was more aligned to absorption in the visible light range used in the study compared to the band gap for 10% F-TiO_2-ZFA (0.9 eV). Dopants may have different effects on the trapping of electrons and holes because of the different positions of the dopants in the TiO_2 crystal lattice.[40] Increasing the content of dopants in TiO_2 introduces defect states which promote electron-hole recombination.[41] Overall, optimising photocatalyst loading is important because it facilitates maximum photocatalytic activity while avoiding unnecessary wastage of photocatalyst.

Photodegradation of E. coli

Because of their superior performance in the photodegradation of MO, the 10% TiO_2-ZFA and 30% F-TiO_2-ZFA photocatalysts were used to remove *E. coli* from water. In the absence of a photocatalyst and in the presence of visible light, 21% disinfection was achieved after 180 min (Figure 7a,b). This can be attributed to photolysis from visible light causing the lysis of the bacterial cells. Previous studies have shown that visible light photolysis alone has a small effect on bacterial inactivation, while the experiment in the dark has been reported to result in no inactivation.[42] The intensity of the LED lights on the photocatalytic reactor may have helped increase the disinfection by photolysis. A disinfection rate of 95% occurred after 3 h of irradiation, while 10% TiO_2-ZFA showed 76% disinfection within 3 h (Figure 7b). This may be due to the higher photocatalytic activity of the co-doped F-TiO_2-ZFA photocatalyst, compared to the singly doped TiO_2-ZFA photocatalyst. Disinfection under visible light was enhanced by the presence of a photocatalyst compared to that in the absence of a photocatalyst. In the presence of a photocatalyst, OH• radicals are formed and released, and these weaken the bacterial cell integrity, leading to loss of cell respiration, and ultimately death.[32] In the presence of a photocatalyst and in the absence of visible light, 37% disinfection was achieved using 30% F-TiO_2-ZFA compared to 29% for 10% TiO_2-ZFA. This disinfection is possibly caused by phagocytosis by the photocatalysts as well as the antimicrobial activity of F^- and TiO_2 nanoparticles, which cause disintegration of the bacterial cell membrane.[43] For the control experiments in the absence of both light and photocatalyst, a mere 3% disinfection was achieved in 180 min. The disinfection could possibly be due to: (1) the absence of a nutrient source for survival of the bacteria, or (2) the antimicrobial activity of nanoparticles. Previous studies have shown that solar energy alone is an effective disinfectant[44], although it requires prolonged exposure. In summary, co-doped 30% F-TiO_2-ZFA has more effective antimicrobial properties due to its higher photocatalytic activity.

Possible photodegradation mechanisms

The photodegradation results show that the photocatalytic efficacy increased in the order: TiO_2< TiO_2-ZFA<F-TiO_2-ZFA. It can thus be deduced that both F and ZFA enhance the photocatalytic properties of TiO_2, possibly via the formation of a hetero-junction between F and TiO_2, and ZFA and TiO_2, which facilitate electron-hole pair separation.[9] Previous studies have reported that F-doping of TiO_2 improved electron trapping, which reduced electron-hole recombination.[8,25] The photodegradation mechanism of MO and *E. coli* using TiO_2-ZFA and F-TiO_2-ZFA can thus be conjectured (Box 1). Upon visible light irradiation, TiO_2 produces electrons and holes, which are respectively entrapped in the photocatalyst and react with H_2O to produce reactive radicals.[8,29] The degradation of MO and *E. coli* is affected by the hydroxyl free radicals to produce by-products and dead biomass, respectively. The degradation mechanism of pathogenic microorganisms can be studied by monitoring the optical density of treated water or by gene expression analyses, and evaluating morphological transformations of cell membranes using microscopy techniques.[45,46] On exposure to light, electron/hole pairs are generated on the photocatalyst surface, leading to a series of reactions facilitated by OH• radicals. These radicals attack *E. coli* cytoplasmic membranes, causing lipid peroxidation and oxidisng the intracellular components, consequently leading to cell death.[45,47]

Conclusion

We investigated the photocatalytic activity and antimicrobial efficacy of TiO_2-ZFA and F-TiO_2-ZFA photocatalysts derived from residues from the combustion of coal. The key findings are:

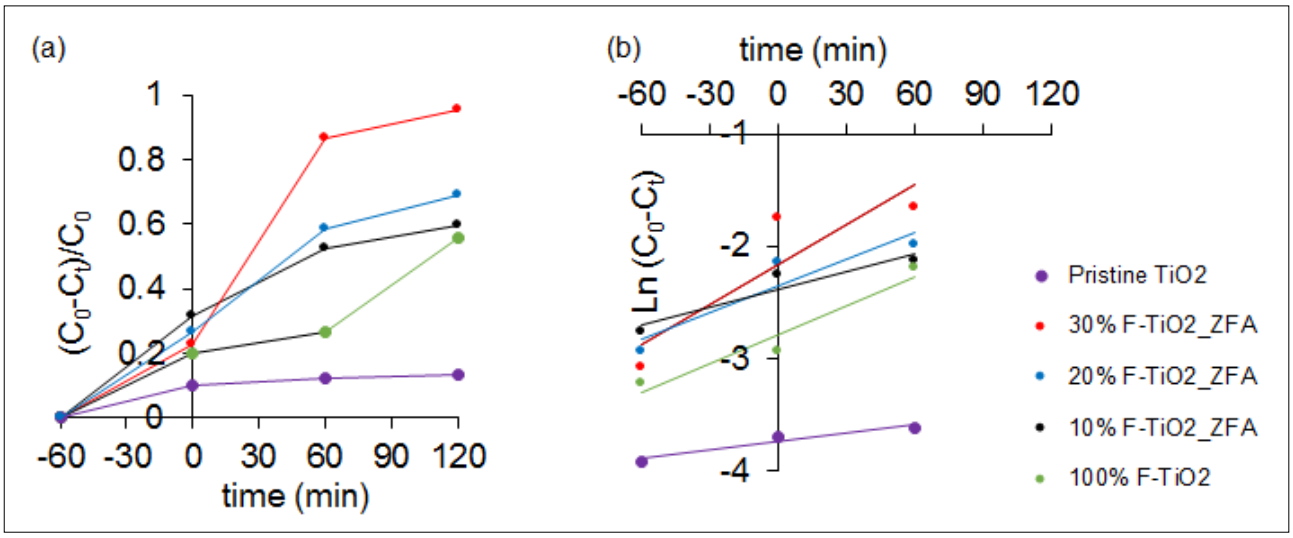

Figure 6: (a) Photodegradation of MO, and (b) pseudo-first-order kinetics using TiO_2 and F-doped photocatalysts.

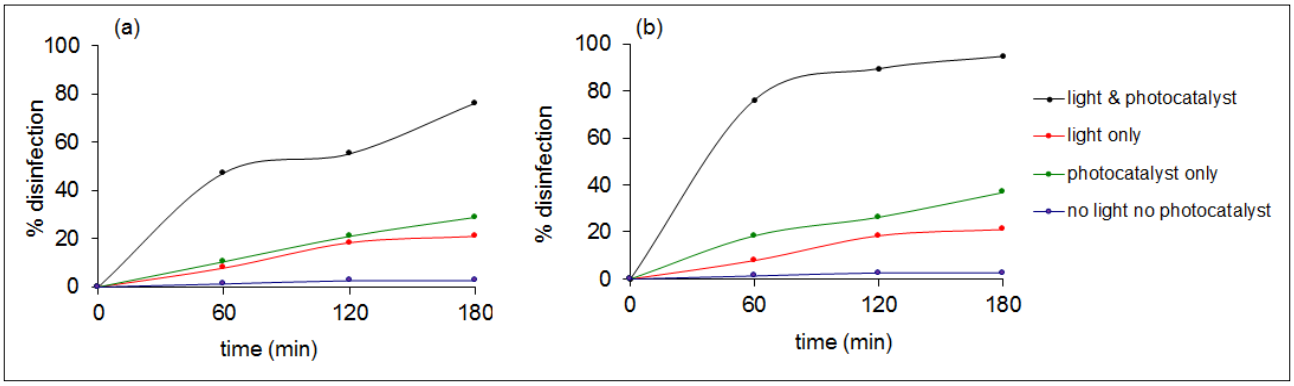

Figure 7: Disinfection studies using average initial viable cell concentration of 3.8 x 10^8 CFU/mL under visible light irradiation of 3 h using (a) 10% TiO_2-ZFA photocatalyst or (b) 10% F-TiO_2-ZFA photocatalyst.

Box 1: Proposed mechanism for the photodegradation of methyl orange (MO) and *Escherichia coli*

$TiO_2 + hv \rightarrow TiO_2^+ + e^-$

$TiO_2^+ \rightarrow TiO_2 + h^+$

F-TiO_2-ZFA + e^- → •F-TiO2-ZFA (e-) (entrapment)

$H_2O + h^+ \rightarrow {}^\bullet OH + H^+$

F-TiO_2-ZFA (e^-) (entrapment) + $O_2 \rightarrow O_2^-$

Degradation of MO

$^\bullet OH + {}^\bullet O_2^- + MO \rightarrow$ Degradates

Degradation of *E. coli*

$^\bullet OH + {}^\bullet O_2^- +$ *E. coli* + water → Disintegration of cell wall

$^\bullet OH$ + cell components → Dead cells

1. FTIR data revealed that F-TiO_2-ZFA photocatalysts had a high content of OH• groups on the surface, which improve the photocatalytic activity of the photocatalysts.
2. F-doped and TiO_2-ZFA photocatalysts showed a 63–72% and 31-38% decrease in the band gap of TiO_2, respectively.
3. F-TiO_2-ZFA photocatalysts had higher disinfection efficacy (95%) than TiO_2-ZFA (76%).
4. MO photodegradation followed pseudo-first-order kinetics.

The performance of photocatalysts was attributed to a combination of the band narrowing effects of the F and ZFA dopants, as well as the adsorption capabilities of the ZFA. The conversion of coal fly ash to photocatalysts has the potential to reduce the environmental impacts associated with the disposal of coal fly ash, while providing novel materials for applications in water and wastewater treatment. In addition, being derived from waste, the material is likely to have lower cost and a reduced environmental footprint relative to commercially available materials. Detailed cost and life-cycle analyses will, however, be useful. Because the technique uses visible light, which is a major component of sunlight, point-of-use devices based on this technique have potential for use in isolated communities. However, large-scale application of this technology is still hindered by the very small particle size of the TiO_2 which poses a challenge for its post-use recovery. A combination of centrifugation, decantation and filtration could be used to recover the nanocomposite in treated water. Because the nanoparticles are usually highly dispersed in aqueous solution, this could limit their recovery and increase the cost of treatment. Besides, the additional processes could increase the cost of the treatment technique. Hence, further studies should investigate up-scaling the technique, investigating the fate of the potential of the photocatalysts for multiple reuse, and the recovery of TiO_2 in treated water. Optimisation studies based on tools such as response surface methodology are also required to develop the best combination of operating conditions. There is also need to investigate methods for the safe disposal of the spent photocatalysts and adsorbents, including their potential use in novel construction materials. Besides using the photocatalysts/adsorbents in free granular form, scope also exists to develop point-of-use water-treatment devices relying on photocatalysis for water disinfection. Recent work involving the development of e-DRINK, a photo-electrocatalytic device for rapid water disinfection, points to the possibility to develop such point-of-use systems. Besides antimicrobial activity, such point-of-use devices should also be tested for their capacity to remove emerging contaminants such as antimicrobials, pharmaceuticals, and pesticides.

Acknowledgements

We are grateful for the technical support from Harare Polytechnic.

Competing interests

We have no competing interests to declare.

Authors' contributions

S.M.M.: Data collection and treatment; manuscript draft writing. N.C.: Conception, supervision, manuscript writing and reviewing. C.I.M.: Supervision, manuscript writing. W.G.: Manuscript writing, reviewing. M.M.: Manuscript writing, materials characterisation. A.T.K.: Manuscript writing, materials characterisation.

References

1. Visa M, Chelaru AM. Hydrothermally modified fly ash for heavy metals and dyes removal in advanced wastewater treatment. Appl Surf Sci. 2014;303:14–22. https://doi.org/10.1016/j.apsusc.2014.02.025
2. Kant R. Textile dyeing industry and environmental hazard. Nat Sci. 2012;4:22–26. https://doi.org/10.4236/ns.2012.41004
3. Ghaly AE, Ananthashanka R, Alhattab M, Ramakrishnan VV. Production, characterization and treatment of textile effluents: A critical review. J Chem Eng Process Technol. 2014;5:1–18. https://doi.org/10.4172/2157-7048.1000182
4. Hao O, Hao OJ, Kim H, Chiang P. Decolorization of wastewater. Crit Rev Environ Sci Technol. 1999;30(4):449–505. https://doi.org/10.1080/10643380091184237
5. Duta A, Visa M. Simultaneous removal of two industrial dyes by adsorption and photocatalysis on a fly-ash-TiO_2 nanocomposite. J Photochem Photobiol A. 2015;306:21–30. https://doi.org/10.1016/j.jphotochem.2015.03.007
6. Martorelli L, Albanese A, Vilte D, Cantet R, Bentancor A, Zolezzi G, et al. Shiga toxin-producing *Escherichia coli* (STEC) O22:H8 isolated from cattle reduces *E. coli* O157:H7 adherence *in vitro* and *in vivo*. Vet Microbiol. 2017;208:8–17. https://doi.org/10.1016/j.vetmic.2017.06.021

7. Rondina DJG, Ymbong DV, Cadutdut MJM, Nalasa JRS, Paradero JB, Mabayo VIF, et al. Utilization of a novel activated carbon adsorbent from press mud of sugarcane industry for the optimized removal of methyl orange dye in aqueous solution. Appl Water Sci. 2019;9:181. https://doi.org/101007/s13201-019-1063-0

8. Mousli F, Chaouchi A, Jouini M, Maurel F, Kadri A, Chehimi MM. Polyaniline-grafted RuO2-TiO_2 heterostructure for the catalysed degradation of methyl orange in darkness. Catalysts. 2019;9(7):578. https://doi.org/10.3390/catal9070578

9. Zarei M, Bahrami J, Zarei M. Zirconia nanoparticle-modified graphitic carbon nitride nanosheets for effective photocatalytic degradation of 4-nitrophenol in water. Appl Water Sci. 2019;9:175. https://doi.org/10.1007/s13201-019-1076-8

10. Gwenzi W, Chaukura N. Organic contaminants in African aquatic systems: Current knowledge, health risks and future research directions. Sci Total Environ. 2018;619–620:1493–1514. https://doi.org/10.1016/j.scitotenv.2017.11.121

11. Pal A, Grain A, Chowdhury D, Mondal MH, Saha B. A comparative spectral study on the interaction of organic dye Congo-Red with selective aqueous micellar media of CPC, rhamnolipids and saponin. Tenside Surf Det. 2020;57(5):401–407. https://doi.org/10.3139/113.110700

12. Mondal MH, Malik S, Saha B. Characterization of pyrene solubilization in selective micellar media of novel bio-degradable natural surfactant saponin (extracted from soap nut) and conventional surfactant SDBS in presence and absence of common salt NaCl. Tenside Surf Det. 2017;54(5):378–384. https://doi.org/10.3139/113.110519

13. Nhapi I, Gijzen HJ. Wastewater management in low-income countries in the context of sustainability. Water Policy. 2004;6(6):501–517. https://doi.org/10.2166/wp.2004.0033

14. Sivalingam S, Sen S. An ultra-fast non-conventional waste management protocol to recycle of industrial fly ash into zeolite X. Environ Sci Pollut Res Int. 2018;26(34):34693–34701. https://doi.org/10.1007/s11356-018-3664-9

15. Koshy N, Singh DN. Fly ash zeolites for water treatment applications. J Environ Chem Eng. 2016;4:1460–1472. http://dx.doi.org/10.1016/j.jece.2016.02.002

16. Taunov Z, Tsakiridis PE, Mikhalovsky SV, Inglezakis VJ. Synthetic coal fly ash-derived zeolites doped with silver nanoparticles for mercury (II) removal from water. J Environ Manage. 2018;224:164–171. https://doi.org/10.1016/j.jenvman.2018.07.049

17. Yahya N, Aziz F, Jamaludin NA, Mutalib MA, Ismail AF, Salleh WNW, et al. A review of integrated photocatalyst adsorbents for wastewater treatment. J Environ Chem Eng. 2018;6(6):7411–7425. https://doi.org/10.1016/j.jece.2018.06.051

18. Liu J, Wang Y, Ma J, Peng Y, Wang A. A review on bidirectional analogies between the photocatalysis and antibacterial properties of ZnO. J Alloy Compd. 2019;783:898–918. https://doi.org/10.1016/j.jallcom.2018.12.330

19. Todorova N, Giannakopoulou T, Vaimakis T, Trapalis C. Structure tailoring of fluorine-doped TiO_2 nanostructured powders. Mat Sci Eng B-Adv. 2008;152:50–54. https://doi.org/10.1155/2008/534038

20. Li J, Liang N, Jin X, Zhou D, Li H, Wu M, et al. The role of ash content on bisphenol A sorption to biochars derived from different agricultural wastes. Chemosphere. 2017;171:66–73. https://doi.org/10.1016/j.chemosphere.2016.12.041

21. Chong MN, Tneu ZY, Poh PE, Jin B, Aryal R. Synthesis, characterisation and application of TiO_2-zeolite nanocomposites for the advanced treatment of industrial dye wastewater. J Taiwan Inst Chem Eng. 2014;50:288–296. https://doi.org/10.1016/j.jtice.2014.12.013

22. Li C, Sun Z, Ma R, Xue Y, Zheng S. Fluorine doped anatase TiO_2 with exposed reactive (001) facets supported on porous diatomite for enhanced visible-light photocatalytic activity. Micropor Mesopor Mat. 2017;243:281–290. https://doi.org/10.1016/j.micromeso.2017.02.053

23. Chang HL, Shih WH. A general method for the conversion of fly ash into zeolites as ion exchangers for cesium. Ind Eng Chem Res. 1998;37:71–78. https://doi.org/10.1021/ie970362o

24. Gwenzi W, Chaukura N, Noubactep C, Mukome FN. Biochar-based water treatment systems as a potential low-cost and sustainable technology for clean water provision. J Environ Manage. 2017;197:32–749. https://doi.org/10.1016/j.jenvman.2017.03.087

25. Mukonza SS, Nxumalo EN, Mamba BB, Mishra AK. Enhanced solar light photodegradation of brilliant black bis-azo dye in aqueous solution by F, Sm^{3+} co-doped TiO_2. IOP Conf Ser Mater Sci Eng. 2017;195:012006. https://doi.org/10.1088/1757-899X/195/1/012006

26. Kausar A, Naeem K, Hussain T, Nazli Z, Bhatti HN, Jubeen F, et al. Preparation and characterization of chitosan/clay composite for direct Rose FRN dye removal from aqueous media: Comparison of linear and non-linear regression methods. J Mater Res Technol. 2019;8(1):1161–1174. https://doi.org/10.1016/j.jmrt.2018.07.020

27. Ferro-Garcia MA, Rivera-Utrilla J, Bautista-Toledo I, Moreno-Castilla C. Adsorption of humic substance on activated carbon from aqueous solutions and their effect on the removal of Cr(III) ions. Langmuir. 1998;14(7):1880–1886. https://doi.org/10.1021/la970565h

28. Kortüm G, Braun W, Herzog G. Principles and techniques of diffuse reflectance spectroscopy. Angew Chem Int Edit. 1963;2(7):333–341. https://doi.org/10.1002/anie.196303331

29. Rosman N, Salleh WNW, Aziz F, Ismail AF, Harun Z, Bahri SS, et al. Electrospun nanofibers embedding ZnO/Ag_2CO_3/Ag_2O heterojunction photocatalyst with enhanced photocatalytic activity. Catalysts. 2019;9:565. https://doi.org/10.3390/catal9070565

30. Yan Y, Zhou X, Lan J, Li Z, Zheng T, Cao W, et al. Efficient photocatalytic disinfection of *Escherichia coli* by N-doped TiO_2 coated on coal fly ash cenospheres. J Photochem Photobiol A. 2018;367:355–364. https://doi.org/10.1016/j.jphotochem.2018.08.045

31. Hassan MA, Nemr AE, Madkour FF. Testing the advanced oxidation processes on the degradation of Direct Blue 86 dye in wastewater. Egypt J Aquat Res. 2017;43(1):11–19. https://doi.org/10.1016/j.ejar.2016.09.006

32. Sreeja S, Shetty VK. Photocatalytic water disinfection under solar irradiation by Ag-TiO_2 core-shell structured nanoparticles. Sol Energy. 2017;157:236–243. https://doi.org/10.1016/j.solener.2017.07.057

33. Ricchiardi G, Damin A, Bordiga S, Lamberti C, Spano G, Rivetti F, et al. Vibrational structure of titanium silicate catalysts. A spectroscopic and theoretical study. J Am Chem Soc. 2001;123:11409–11419. https://doi.org/10.1021/ja010607v

34. Larkin P. General outline and strategies for IR and Raman spectral interpretation. In: Larkin P, editor. Infrared and Raman spectroscopy: Principles and spectral interpretation. Elsevier; 2011. p. 117–133.

35. An C, Yang S, Huang G, Zhao S, Zhang P, Yao Y. Removal of sulfonated humic acid from aqueous phase by modified coal fly ash waste: Equilibrium and kinetic adsorption studies. Fuel. 2016;165:264–271. https://doi.org/10.1016/j.fuel.2015.10.069

36. Ndlangamandla NG, Kuvarega AT, Msagati TAM, Mamba BB, Nkambule TTI. A novel photodegradation approach for the efficient removal of natural organic matter (NOM) from water. Phys Chem Earth. 2018;106:97–106. https://doi.org/10.1016/j.pce.2018.05.011

37. Busca G. Catalytic materials based on silica and alumina: Structural features and generation of surface acidity. Prog Mater Sci. 2019;104:215–249. https://doi.org/10.1016/j.pmatsci.2019.04.003

38. Umadevi M, Parimaladevi R, Sangari M. Synthesis, characterisation and photocatalytic activity of fluorine doped TiO_2 nanoflakes synthesized using solid state reaction method. Spectrochim Acta A Mol Biomol Spectrosc. 2014;120:365–369. https://doi.org/10.1016/j.saa.2013.10.046

39. Li FB, Li XZ, Ao CH, Lee SC, Hou MF. Enhanced photocatalytic degradation of VOCs using Ln^{3+}-TiO_2 catalysts for indoor air purification. Chemosphere. 2005;59(6):787–800. https://doi.org/10.1016/j.chemosphere.2004.11.019

40. Manusamy S, Aparna RSI, Prasad RGSV. Photocatalytic effect of TiO_2 and the effect of dopants on degradation of brilliant green. Sustain Chem Process. 2013;1:4. https://doi.org/10.1186/2043-7129-1-4

41. Ozawa K, Emori M, Yamamoto S, Yukawa R, Yamamoto S, Hobara R, et al. Electron-hole recombination time at TiO_2 single-crystal surfaces: Influence of surface band bending. J Phys Chem Lett. 2014;5(11):1953–1957. https://doi.org/10.1021/jz500770c

42. Booshehri AY, Polo-Lopez MI, Castro-Alferez M, Pengfie-He Rong X, Rong W, Malato S, et al. Assessment of solar photocatalysis using Ag/$BiVO_4$ at pilot solar compound parabolic collector for inactivation of pathogen in well water and secondary effluents. Catalysis. 2017;281(1):124–134. https://doi.org/10.1016/j.cattod.2016.08.016

43. Wang L, Hu C, Shao L. The antimicrobial activity of nanoparticles: Present situation and prospects for the future. Int J Nanomedicine. 2017;12:1227–1249. https://doi.org/10.2147/IJN.S121956

44. Pichel N, Vivar M, Fuentes M. The problem of drinking water access: A review of disinfection technologies with an emphasis on solar treatment methods. Chemosphere. 2019;218:1014-1030. https://doi.org/10.1016/j.chemosphere.2018.11.205

45. Alafif ZO, Anjum M, Ansari,MO, Kumar R, Rashid J, Madkour M, Barakat MA. Synthesis and characterization of S-doped-rGO/ZnS nanocomposite for the photocatalytic degradation of 2-chlorophenol and disinfection of real dairy wastewater. J Photochem Photobiol A Chem. 2019;377:190–197. https://doi.org/10.1016/j.jphotochem.2019.04.004

46. Li Y, Zhao J, Zhang G, Zhang L, Ding S, Shang E, et al. Visible-light-driven photocatalytic disinfection mechanism of PB-$BiFeO_3$/rGO photocatalyst. Water Res. 2019;161:251–261 https://doi.org/10.1016/j.watres.2019.06.011

47. Arellano U, Asomoza M, Ramírez F. Antimicrobial activity of Fe–TiO_2 thin film photocatalysts. J Photochem Photobiol A Chem. 2011;222:159–165. https://doi.org/10.1016/j.jphotochem.2011.05.016